CIRP Annals - Manufacturing Technology 00 (2026) 1–5

Contents lists available at ScienceDirect

CIRP Annals - Manufacturing Technology

journal homepage: https://www.editorialmanager.com/CIRP/default.aspx

Near-field acoustic gripping for contactless semiconductor die handling

Yaoke Wang[a], Ziming Zhao[a], Yi Shi[b], Ping Guo (2)[a,*]

[a] Department of Mechanical Engineering, Northwestern University, Evanston, IL 60208, USA
[b] Technology Research, Intel Corporation, Chandler, AZ 85226, USA

ARTICLE INFO

Article history:
Available online xxx

Keywords:
Handling
Ultrasonic
Near-field acoustic

ABSTRACT

This study presents near-field acoustic gripping for contactless semiconductor die handling. Existing near-field acoustic attraction fails for larger objects because repulsive squeeze pressure overwhelms attractive edge effects. A mechanistic model resolving these competing forces is presented to explain the geometric size constraint. To address the size limitation, a scalable multi-island design that segments the air film is proposed to maintain the attractive regime. Experiments demonstrate stable pickup of an 8 by 8 millimeter silicon die, doubling the known size limit. The system achieves a high vertical stiffness of 522 N/m and withstands 0.7 g lateral acceleration, validating its potential for advanced packaging.

1. Introduction

Advanced semiconductor packaging processes, particularly hybrid bonding, impose increasingly stringent requirements on particle-free die handling. As interconnect dimensions shrink to the sub-10 μm scale, even minute contamination at the bonding interface can result in catastrophic yield loss. Conventional contact-based handling methods, including mechanical grippers and vacuum pickup, inevitably introduce contamination transfer between dies, potential nozzle wear and surface damage, and particle generation induced by pneumatics. Particulate contamination represents the dominant failure mechanism in integrated circuit fabrication [1]. This challenge is further exacerbated as semiconductor dies become thinner and smaller, where mechanical contact not only generates particles but also risks fracture and surface damage [2].

Existing contactless handling techniques have critical limitations for semiconductor die applications. Bernoulli grippers utilize airflow-induced pressure differences to achieve non-contact pickup, but they suffer from poor lateral positional stability and may generate turbulent flow that entrains particle contamination [3,4]. Magnetic levitation systems can, in principle, provide full six-degree-of-freedom control, but they require magnetic materials, active control architectures, and substantial power consumption, making them impractical for semiconductor die handling [5,6].

NFAL offers a promising contactless handling alternative due to its material-independent operation, inherently passive self-stabilization [7], and compatibility with flat objects in transport applications [8,9]. In NFAL, ultrasonic vibration generates a thin air film with periodic oscillatory flow between the vibrating surface and the object. The nonlinear behavior of this confined air film produces a biased time-averaged thrust force, which in conventional NFAL configurations generates a repulsive force that supports objects from below [10,11].

When the object is placed beneath the vibration surface under a stringent geometric condition, NFAL can generate a net attractive force to suspend objects against gravity, potentially offering a completely non-contact gripping solution ideal for semiconductor die handling. This specific geometric regime requires the lateral dimension of the object to be smaller than the acoustic wavelength, typically less than 4 mm at 21 kHz [12]. This size constraint arises from the competition between the squeeze and edge effects within the air film, but prior work on these effects [13] was conducted in the conventional levitation (repulsion) context, where the edge effect acts as a boundary pressure drop that partially reduces the net repulsive force, but never produces attraction. Their competing roles in the attractive regime, and the connection to the geometric size constraint, remain unexplored. Due to this limited understanding, very few studies have effectively demonstrated the attractive phenomenon [12,14], and all are restricted to object sizes below 4 mm. This falls short of the 4–16 mm die sizes required in contemporary packaging, representing a critical barrier to industrial adoption.

To address these knowledge gaps, a mechanistic model is established that clarifies the competing nature of the repulsive squeeze effect and the attractive edge effect within the air film. This model provides the physical explanation for the transition between attraction and repulsion, as well as the fundamental reason for the size constraint. Air film segmentation is proposed as a scalable design strategy to decouple attraction generation from object size, thereby overcoming the critical size barrier identified in previous studies.

This approach is implemented using a multi-island architecture, where four islands independently generate gripping force to collectively suspend larger objects. The first demonstration of near-field acoustic gripping for dies up to 8 × 8 mm is presented, effectively doubling the previously known size limit [12,14].

* Corresponding author.
E-mail address: ping.guo@northwestern.edu (P. Guo).

https://doi.org/10.1016/j.cirp.2026.04.022

Please cite this article as: Y. Wang et al., Near-field acoustic gripping for contactless semiconductor die handling, CIRP Annals - Manufacturing Technology (2026), https://doi.org/10.1016/j.cirp.2026.04.022

2. Mechanistic modeling of near-field acoustic gripping

The generation of attractive force in near-field acoustic gripping is not a unitary phenomenon, but rather the result of a dynamic equilibrium between competing pressure distributions. As illustrated in Fig. 1(a), when the vibrating head oscillates, two distinct flow mechanisms emerge: a repulsive squeeze effect driven by inertial flow at the center, where air is compressed and expelled, and a viscous attractive edge effect. To explain the physical origin of the size constraint, a mechanistic model is established that resolves the air film dynamics into these two components.

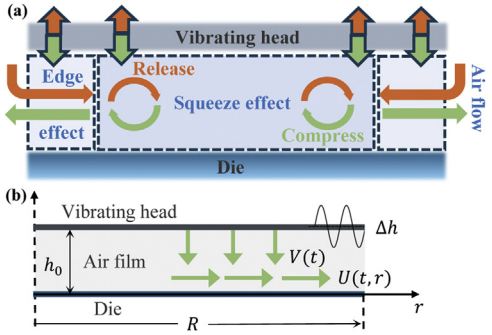

Fig. 1. (a) Schematic of near-field acoustic gripping of a semiconductor die; and (b) axisymmetric model for analyzing the dual squeeze-edge effect.

To derive the governing equations for both the squeeze and edge effects, an axisymmetric configuration is assumed, consisting of a circular vibrating source and a parallel planar object beneath it. As shown in Fig. 1(b), the system geometry is defined by the effective radius R and the mean air film thickness h_0. The kinematics of the air film are governed by the transducer vibration, characterized by angular frequency ω, amplitude Δh, and vertical velocity $V(t)$, which drives a corresponding radial airflow velocity $U(r,t)$. The fluid is modeled with density ρ. The core formulation of the mechanistic model is presented here, while detailed derivations are provided in the Supplementary Materials.

In the operating regime relevant to this study ($h_0 \ll R$ with a high squeeze number), the squeeze effect is dominated by inertial flows. Consequently, the following derivation assumes an inviscid, inertia-dominated flow regime. First, the conservation of mass relates the radial airflow velocity, $U(r,t)$, to the vibration head velocity, $V(t) = \Delta h\omega\cos(\omega t)$. Second, the pressure gradient is governed by the inviscid momentum balance. These governing relationships are expressed as:

$$\text{Continuity}: \ U(r,t) = -\frac{r}{2h_0}V(t), \tag{1}$$

$$\text{Momentum}: \rho\frac{\partial U}{\partial t} + \rho U\frac{\partial U}{\partial r} = -\frac{\partial p(r,t)}{\partial r}. \tag{2}$$

The edge effect is modeled using rectified boundary conditions. During the compress phase, the outflow air encounters minimal resistance, and the boundary pressure approximates atmospheric pressure. In contrast, during the release phase, the rapid acceleration of inflow air at the gap entrance induces a pressure drop at the perimeter [13]. These conditions are expressed as:

$$p(R,t) = \begin{cases} 0 & \text{compress phase} \\ -\Delta P_{edge} & \text{release phase} \end{cases}, \tag{3}$$

The edge pressure drop is related to a viscous friction, or a linear drag rather than inertia when the air film h_0 is very small with high vibration frequency. The dimensional analysis indicates a linear relationship between the pressure drop and edge air velocity. By considering a local active length L_{local} near the gap entrance, the air velocity at the edge can be estimated as:

$$U(R,t) = \frac{L_{local}}{h_0}(\Delta h\omega)cos(\omega t), \tag{4}$$

where the length L_{local} is related to the local edge geometry and vibration frequency through the scaling law, $L_{\text{local}} \propto 1/\sqrt{\omega}$. The average pressure drop over one cycle then can be estimated as:

$$\overline{\Delta P_{\text{edge}}} \approx \frac{\beta(h_0)\sqrt{\omega}\Delta h}{\pi h_0}, \tag{5}$$

where β is a resistance coefficient that depends on the local edge geometry. A quadratic relationship between the air film thickness and β is assumed.

Substituting Eq. (1) into Eq. (2), integrating over r, and averaging over one cycle (the local acceleration $\partial U/\partial t$ term vanishes), the cycle-averaged pressure distribution is obtained as:

$$\overline{p}(r) = \underbrace{K\cdot\frac{\rho\omega^2(\Delta h)^2}{16h_0^2}\left(R^2-r^2\right)}_{\text{Inertial Squeeze Effect}} \underbrace{-\beta(h_0)\cdot\frac{\sqrt{\omega}\Delta h}{2\pi h_0}}_{\text{Viscous Edge Effect}}, \tag{6}$$

where K is introduced as an inertial profile correction factor [15]. Both K and $\beta(h_0)$ are fitted from simulation results and listed in Table 1. Finally, the net force F_{net} acting on the object is derived by integrating Eq. (6) over the effective area:

$$F_{\text{net}} = \int_0^R \overline{p}(r)2\pi r\mathrm{d}r = K\frac{\rho\omega^2(\Delta h)^2}{32h_0^2}R^4 - \beta\frac{\sqrt{\omega}\Delta h}{2\pi h_0}\pi R^2 \tag{7}$$

Model validation. The analytical results were validated against full-scale computational fluid dynamics (CFD) simulations performed in ANSYS CFX using a three-dimensional compressible flow model. The simulation geometry replicates the model configuration shown in Fig. 1(b), with the top plate executing sinusoidal oscillations while the bottom die surface remains stationary. Each simulation spanned 20 complete oscillation cycles with a time step of 2 μs, providing 30 data points per cycle. The pressure field was time-averaged over the final five cycles to ensure the capture of the steady-state response after initial transients decayed. All model parameters align with the values listed in Table 1.

Table 1
Model parameter ranges.

Radius $R = 1.1 \sim 1.7$ mm	Vibration amplitude $\Delta h = 10$ μm
Air film thickness $h_0 = 10 \sim 100$ μm	Air Density $\rho = 1.225$ kg/m^3
Angular frequency ω = 188,495 rad/s (30 kHz)	Inertial factor K (fitted, global) 4.31
Resistance coefficient $\beta(h_0)$ (fitted, typical range: 5~35) $\beta(h_0) = -0.024h_0^2 + 2.236h_0 - 14.87$ (h_0 is expressed in μm)	

Validation focused on a die radius of R = 1.3 mm with air film thicknesses ranging from 40 μm to 55 μm, as shown in Fig. 2(a). A comparison of simulated pressure profiles (solid curves) and model predictions (dashed curves) reveals normalized mean errors of 3.49% (40 μm), 5.26% (45 μm), 22.63% (50 μm), and 20.92% (55 μm). The agreement is particularly strong in the central positive-pressure zone. Discrepancies increase near the periphery, indicating that the edge resistance coefficient β has a more complex dependence on boundary geometry. Nevertheless, the mechanistic model successfully captures the critical transition from the repulsive squeeze effect to the attractive edge effect. A sensitivity analysis of the key model parameters (K, β, Δh, and ω) is provided in the Supplementary Materials. The net force is most sensitive to the edge resistance coefficient β (±29% per ±20% perturbation), while the critical radius is primarily governed by the angular frequency ω. These results confirm that the model predictions are robust within the experimentally relevant parameter ranges.

Competing mechanisms and size limitation. As Eq. (6) shows, the center exhibits a positive pressure dominated by the inertial squeeze effect, while the pressure transitions to negative near the boundary due to the viscous edge effect (Fig. 2(a), R = 1.3 mm).

Please cite this article as: Y. Wang et al., Near-field acoustic gripping for contactless semiconductor die handling, CIRP Annals - Manufacturing Technology (2026), https://doi.org/10.1016/j.cirp.2026.04.022

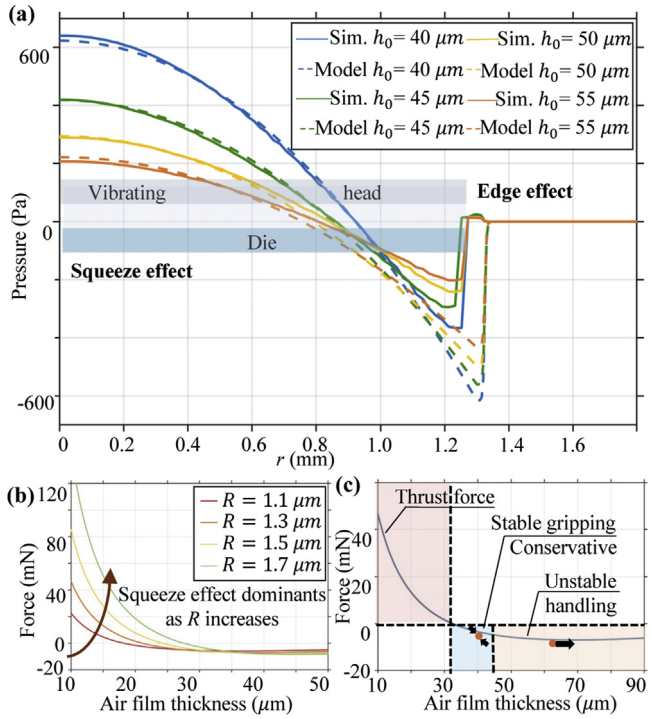

Fig. 2. (a) Comparison of CFD simulation (solid) with analytical model predictions (dashed); (b) size-dependent effect showing the attraction to repulsion transition based on radius R; and (c) net force curve revealing three operating regimes: contact prevention, stable gripping, and unstable handling.

The net force equation in Eq. (7) reveals the fundamental physical origin of the size barrier in near-field acoustic gripping. The repulsive squeeze force scales with the fourth power of the radius (R^4), while the attractive force scales only with the square of the radius (R^2). As shown in Fig. 2(b), when R increases, the repulsive component shifts the entire curve upward. Beyond a critical radius, the attractive force region disappears entirely, transitioning the system to a purely repulsive mode.

Stable pickup regime. For practical handling, the system must not only generate a net lifting force but also provide a stable equilibrium position. With the object size R fixed, the net force equation reveals another critical scaling distinction regarding the air film h_0. The repulsive squeeze force scales with $1/h_0^2$, while the attractive force scales with $1/h_0$. As shown in Fig. 2(c), this interaction creates a potential well analogous to interatomic van der Waals forces, leading to three distinct operating regimes. At small gaps, the $1/h_0^2$ dependence of the squeeze effect creates strong short-range repulsion that prevents contact damage. As the gap increases, the system enters a stable gripping regime where the edge effect dominates. In this region, the net force is attractive (gripping force), and the force gradient is negative, providing a positive stiffness that restores the object to equilibrium against disturbances. When a disturbance pushes the die closer (h_0 decreases), the force moves up the curve into the positive (thrust) region to push back the die. When a disturbance pulls the die away (h_0 increases), the force moves down the curve into the deeper negative (attraction) region, so the die is pulled back up. However, when the gap exceeds a critical value, this restoring capability diminishes, rendering the object susceptible to fall-off.

Model limitations. First, the incompressible flow assumption may become inaccurate at very high vibration amplitudes where compressibility effects are non-negligible. Second, the resistance coefficient β is empirically fitted over a finite range of air film thicknesses (10–100 μm); the increased discrepancy at h_0 = 50–55 μm (Fig. 2(a)) suggests that the edge loss mechanism and the viscosity impact have a more complex dependence on boundary geometry than captured by the current quadratic fit. Finally, thermal dissipation at the gap boundary and acoustic streaming are also outside the scope of the current model.

3. Scalable design via air-film segmentation

The theoretical framework in Section 2 identifies the effective radius R_{eff} as the governing constraint, where $R_{\text{eff}} = \sqrt{A/\pi}$ for rectangular dies. Because the derivation assumes axisymmetric geometry, CFD simulations were performed to compare circular and equal-area square configurations. The circular case produces a 19% larger attractive force due to its smooth curvature (zero vertices), confirming that the axisymmetric model provides an upper bound for rectangular dies. Regardless of the cross-sectional shape, however, because the repulsive squeeze term ($\propto R^4$) inherently overwhelms the attractive edge term ($\propto R^2$) at large scales, parameter tuning (e.g., increasing frequency or amplitude) yields diminishing returns. Consequently, the only fundamental solution is to reduce the effective length scale of the interaction.

To achieve this, Air-film segmentation is introduced as a scalable design strategy: by partitioning the pickup head into a multi-island array, the edge effect is amplified while decoupling the attraction mechanism from the object's total footprint. Specifically, to pick up an 8 × 8 mm die (0.775 mm in thickness and 0.11 grams in weight), the vibration head surface is divided into four independent 3.2 × 3.2 mm sub-islands separated by 1.6 mm wide isolation channels, as shown in Fig. 3. This architecture reduces the effective radius of each interaction zone from $R_{\text{eff}} \approx 4.5$ mm (full die) to $R_{\text{eff}} \approx 1.8$ mm for each island. According to the size dependence map in Fig. 2(c), this design successfully shifts the operation to the attractive regime needed for a stable pickup.

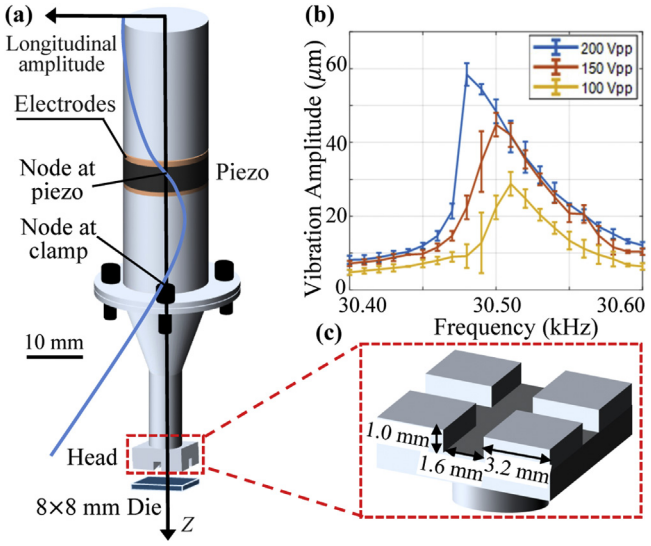

Fig. 3. (a) Schematic of the transducer design of the pickup head; (b) measured head vibration amplitudes under different excitation conditions; and (c) detailed view of the segmented multi-island head design.

To drive the segmented head with sufficient acoustic energy, a custom Langevin-type ultrasonic transducer was designed and fabricated, as shown in Fig. 3(a) with the detailed head design shown in Fig. 3(c). The assembly consists of a piezoelectric stack clamped between a metal back mass and a front horn, where the cross-sectional area tapers toward the tip to function as a mechanical amplifier. The geometry was optimized via finite element simulation to establish a pure longitudinal vibration mode with displacement nodes at the piezoelectric stack and mounting flange. This configuration enables maximum vibration amplitude at the head while minimizing vibration transmission to the fixtures. The final fabricated device operates at a resonance frequency of 30.5 kHz and is capable of generating stable vibration amplitudes up to 30 μm under a 200 Vpp excitation shown in Fig. 3(b).

The vertical net force was characterized using a precision weight scale (1 mg resolution). The air film thickness was varied quasi-statically using a manual precision stage. The measured force–gap relationships under different vibration amplitudes are presented in

Please cite this article as: Y. Wang et al., Near-field acoustic gripping for contactless semiconductor die handling, CIRP Annals - Manufacturing Technology (2026), https://doi.org/10.1016/j.cirp.2026.04.022

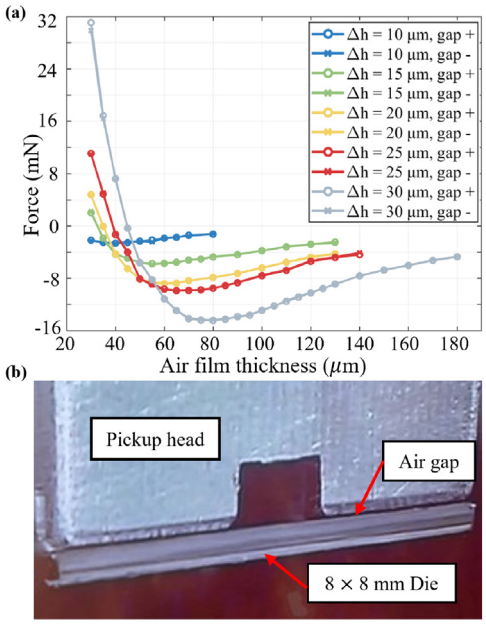

Fig. 4. (a) Measured near-field acoustic force (positive as thrust and negative as the attraction). The solid lines (gap+) report the force measured in the increase direction of the air gap, while the dashed lines (gap-) are measured when the air gap is decreasing. (b) Experimental photo of an 8 × 8 mm silicon die gripped by the system with an air gap.

Fig. 4(a). The vertical stiffness in the stable gripping region, calculated from the slope of the force-gap curve, was estimated to be 522 N/m.

The measured force–gap curves (Fig. 4(a)) confirm the predicted transition from repulsion to attraction. The maximum pickup force of 15 mN exceeds the die weight (1.1 mN) by over 10×, demonstrating ample margin for industrial handling. Furthermore, the excellent overlap between gap expansion (gap+) and contraction (gap-) profiles confirms negligible hysteresis. A photograph of the successful contactless gripping of an 8 × 8 mm die is shown in Fig. 4(b), where a visible air gap is observed between the two surfaces. A supplementary movie S1 is provided to demonstrate the complete pickup process.

4. Lateral stability and stiffness characterization

For precision contactless handling, the system must constrain the object not only vertically but also laterally. The mechanistic model established in Section 2 predicts that the time-averaged pressure distribution follows a parabolic profile, with maximum repulsion at the center decreasing to negative attraction at the periphery. This non-uniform pressure field naturally generates a radial restoring force that self-centers the object.

To quantify this stability, the residual lateral oscillation of the die was analyzed while in the suspended state. A laser Doppler vibrometer (Polytec NLV-2500, Germany) was used to record the vibratory motion of the die edge. The measured oscillation amplitudes in the lateral direction fall within 1–5 μm with no evident dependence on the operating parameters (excitation voltage). However, as shown in Fig. 5(a), the residual oscillation frequency increases with the excitation voltage, ranging from 4 to 16 Hz. The lateral stiffness was derived from this characteristic frequency using a mass-spring model, reaching a maximum of 1.1 N/m. The results show that stiffness increases non-linearly with the vibration amplitude, indicating that increasing the acoustic power not only strengthens the vertical attraction but also tightens the lateral confinement. Lateral stability under dynamic conditions was further validated by mounting the system on a reciprocating linear stage (Aerotech PRO165LM, USA); stable gripping was maintained up to 0.7 g before die drop-off.

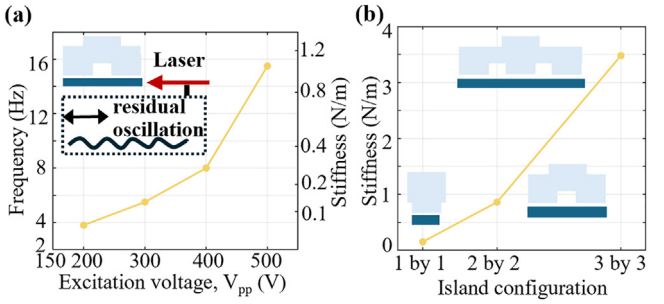

Fig. 5. (a) Measured characteristic frequencies of lateral oscillation and corresponding lateral stiffness at different excitation voltages; (b) simulated lateral stiffness for 1 by 1, 2 by 2, and 3 by 3 island configurations.

To further investigate how lateral stiffness scales with the number of islands, CFD simulations were performed in ANSYS CFX for 1 by 1, 2 by 2, and 3 by 3 configurations, corresponding to 1, 4, and 9 islands. The detailed simulation setup and results are provided in the Supplementary Materials. All simulations were conducted at an air gap of h_0 = 50 μm and vibration amplitude of Δh = 10 μm. As shown in Fig. 5(b), lateral stiffness scales superlinearly with island count: 0.15 N/m for a single island, 0.86 N/m for the four-island array (comparable to 1.1 N/m obtained from the experiment), and 3.48 N/m for the nine-island array, with the increase exceeding simple proportionality.

5. Conclusion

This study overcomes the geometric constraints limiting near-field acoustic gripping. The mechanistic model reveals that performance depends on the competition between repulsive inertial forces (scaling with R^4) and attractive edge forces (scaling with R^2). These forces scale differentially with air film thickness, creating a "potential well" regime that ensures self-stable equilibrium. Leveraging these insights, a multi-island architecture was proposed and validated that decouples the attraction mechanism from the object's footprint. This design successfully suspended an 8 × 8 mm silicon die, doubling the previously known size limit. The system achieved a holding force of 15 mN, a vertical stiffness of 522 N/m, a lateral stiffness of 1.1 N/m, and pickup stability under 0.7 g lateral acceleration. Future work will focus on scaling to full wafers and enhancing lateral stiffness. This work suggests the feasibility of a passive, contamination-free solution for next-generation semiconductor handling.

CRediT authorship contribution statement

Yaoke Wang: Writing – original draft, Visualization, Validation, Methodology, Investigation, Formal analysis. **Ziming Zhao:** Writing – original draft, Visualization, Validation, Methodology, Investigation, Formal analysis. **Yi Shi:** Writing – review & editing, Methodology, Funding acquisition, Conceptualization. **Ping Guo (2):** Writing – review & editing, Methodology, Funding acquisition, Conceptualization, Resources, Supervision.

Acknowledgments

This work was supported by Intel Corporation, under grant number Intel CG# 93669185. The authors gratefully acknowledge Charles El Helou and Sheena Benson (Technology Research, Intel Corporation) for their valuable discussions and contributions.

Supplementary materials

Supplementary material associated with this article can be found in the online version at doi:10.1016/j.cirp.2026.04.022.

References

[1] Otoko JA (2025) Microelectronics Cleanroom Design: Precision Fabrication For Semiconductor Innovation, AI, and National Security in the U.S. Tech Sector. *International Research Journal of Modernization in Engineering Technology and Science* 7 (2):1833–1852.
[2] Shu L, Li C, Wu Y, Hang T, Liu L, Li M (2024) The Influence of Sub-Surface Damage Microstructure on Ultra-Thin Die Flexural Strength. *Journal of Materials Research and Technology* 32:2716–2727.
[3] Liu D, Liang W, Zhu H, Teo CS, Tan KK (2017) Development of a Distributed Bernoulli Gripper for Ultra-Thin Wafer Handling. In: *Proceedings of the 2017 IEEE International Conference on Advanced Intelligent Mechatronics (AIM)*, IEEE, Munich, Germany, 265–270.
[4] Wang S, Wang Y, Mei D, Dai S (2021) Development of an Annular-Shaped Bernoulli Gripper for Contactless Gripping of Large-Size Silicon Wafer. In: *Proceedings of the 2021 IEEE 16th International Conference on Nano/Micro Engineered and Molecular Systems (NEMS)*, IEEE, Xiamen, China, pp. 1871–1876.
[5] Lu X, Usman I, Trumper DL (2012) 6D Direct-Drive Technology for Planar Motion Stages. *CIRP Annals - Manufacturing Technology* 61(1):359–362.
[6] Zhu Z, Chen L, To S (2021) A Novel Direct Drive Electromagnetic XY Nanopositioning Stage. *CIRP Annals - Manufacturing Technology* 70(1):415–418.
[7] Wang F, et al. (2025) Near-Field Acoustic Levitation Generated by Dual-Frequency Ultrasound. *Sensors and Actuators A: Physical* 381:116079.
[8] Liu Y, Sun X, Zhao Z, Zeng H, Chen W (2024) Stability Analysis of Near-Field Acoustic Levitation Considering Misalignment and Inclination. *International Journal of Mechanical Sciences* 264:108832.
[9] Li W, Zhang P, Yang S, Cai S, Feng K (2024) A Novel Two-Dimensional Non-Contact Platform Based on Near-Field Acoustic Levitation. *International Journal of Mechanical Sciences* 265:108865.
[10] Li W, et al. (2023) A Novel Non-Contact Carrying and Transportation Method Based on Near-Field Acoustic Levitation and Negative Pressure Adsorption. *Sensors and Actuators A: Physical* 351:114163.
[11] Wang Y, Guo P (2021) Stiffness Modeling for Near Field Acoustic Levitation Bearings. *Applied Physics Letters* 118(20):204102.
[12] Andrade MA, Ramos TS, Adamowski JC, Marzo A (2020) Contactless Pick-and-Place of Millimetric Objects Using Inverted Near-Field Acoustic Levitation. *Applied Physics Letters* 116(5):054104.
[13] Li J, Cao W, Liu P, Ding H (2010) Influence of Gas Inertia and Edge Effect on Squeeze Film in Near Field Acoustic Levitation. *Applied Physics Letters* 96(24): 243507.
[14] Yoshimoto S, Shou T, Somaya K (2013) Vertical Attractive Force Generated in a Noncontact Chuck Using Ultrasonic Vibration. *Precision Engineering* 37 (4):805–811.
[15] Tichy JA (1981) An Approximate Analysis of Fluid Inertia Effects in Axisymmetric Laminar Squeeze Film Flow at Arbitrary Reynolds Number. *Applied Scientific Research* 37:301–312.

Please cite this article as: Y. Wang et al., Near-field acoustic gripping for contactless semiconductor die handling, CIRP Annals - Manufacturing Technology (2026), https://doi.org/10.1016/j.cirp.2026.04.022